Polydopamine-modified chitin conduits with sustained release of bioactive peptides enhance peripheral nerve regeneration in rats

Ci Li[1, 2, 3, #], Song-Yang Liu[1, 2, 3, #], Li-Ping Zhou[4, #], Tian-Tian Min[4], Meng Zhang[1, 2, 3], Wei Pi[1, 2], Yong-Qiang Wen[4, *], Pei-Xun Zhang[1, 2, 3, *]

Graphical Abstract *Construction and application of polydopamine-modified chitin conduits loaded with mimetic peptides (Chi/PDA-Ps) in a rat model of peripheral nerve injury*

Chi/PDA-Ps conduit   RGI   KLT   SCs   HUVECs
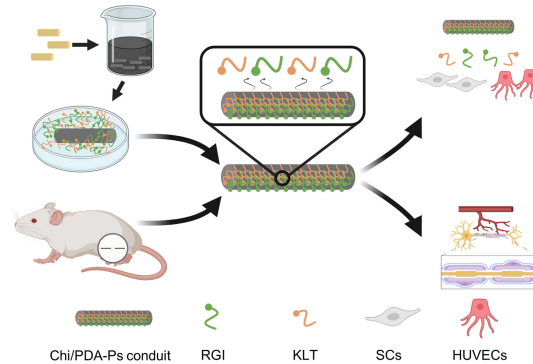
Abstract

The introduction of neurotrophic factors into injured peripheral nerve sites is beneficial to peripheral nerve regeneration. However, neurotrophic factors are rapidly degraded *in vivo* and obstruct axonal regeneration when used at a supraphysiological dose, which limits their clinical benefits. Bioactive mimetic peptides have been developed to be used in place of neurotrophic factors because they have a similar mode of action to the original growth factors and can activate the equivalent receptors but have simplified sequences and structures. In this study, we created polydopamine-modified chitin conduits loaded with brain-derived neurotrophic factor mimetic peptides and vascular endothelial growth factor mimetic peptides (Chi/PDA-Ps). We found that the Chi/PDA-Ps conduits were less cytotoxic *in vitro* than chitin conduits alone and provided sustained release of functional peptides. In this study, we evaluated the biocompatibility of the Chi/PDA-Ps conduits. Brain-derived neurotrophic factor mimetic peptide and vascular endothelial growth factor mimetic peptide synergistically promoted proliferation of Schwann cells and secretion of neurotrophic factors by Schwann cells and attachment and migration of endothelial cells *in vitro*. The Chi/PDA-Ps conduits were used to bridge a 2 mm gap between the nerve stumps in rat models of sciatic nerve injury. We found that the application of Chi/PDA-Ps conduits could improve the motor function of rats and reduce gastrocnemius atrophy. The electrophysiological results and the microstructure of regenerative nerves showed that the nerve conduction function and remyelination was further restored. These findings suggest that the Chi/PDA-Ps conduits have great potential in peripheral nerve injury repair.

Key Words: angiogenesis; bioactive peptides; nerve repair; neurotrophic factor; peripheral nerve injury; peripheral nerve regeneration; polydopamine; surface modification; synergistic effects; tissue engineering

Introduction

Peripheral nerve injury (PNI) is a global clinical problem characterized by partial or complete loss of sensory, motor, or autonomic functions. Neuropathic pain is a common complication of PNI that adversely affects patients physically and psychologically and creates economic burdens on individuals and society (Jiang et al., 2017). The small gap conduit suture technique can be used to substitute traditional epineurium neurorrhaphy to repair PNI (Rao et al., 2019). However, chitin (Chi) conduits stand out among various types of nerve conduits for use in PNI repair because of their ease of synthesis (Younes and Rinaudo, 2015; Riaz Rajoka et al., 2020). The use of biodegradable Chi conduits combined with tubulization can improve the accuracy of axonal docking, reduce the incidence of neuroma, and shorten operation times (Kou et al., 2013; Zhang et al., 2013).

Brain-derived neurotrophic factor (BDNF) and vascular endothelial growth factor (VEGF) provide a microenvironment that is beneficial for peripheral nerve regeneration (Guaiquil et al., 2014; Lopes et al., 2017; Xia and Lv, 2018). Recently, certain bioactive peptides have been substituted for growth factors such as BDNF and VEGF. These mimetic peptides are based on the original growth factors, but with simplified sequences and structures, and they retain the ability to activate the equivalent receptors (D'Andrea et al., 2005; Rubert Pérez et al., 2017; Lu et al., 2018). Herein, we used the neurotrophic peptide sequence RGIDKRHWNSQ (RGI) to mimic BDNF function and the motif KLTWQELYQLKYKGI (KLT) as a VEGF mimetic peptide (Rao et al., 2020).

To obtain optimal biological efficacy of the RGI and KLT mimetic peptides, we developed a self-polymerization method to modify Chi conduits and then combined the mimetic peptides into a system that provides sustained release of these peptides. The outstanding properties of polydopamine (PDA),

including remarkable biocompatibility and superior adhesion, have qualified it for a wide range of biomaterial applications (Liu et al., 2014; Cheng et al., 2019). Compared with other physical adsorption strategies, PDA provides an easier and more efficient method of coating Chi conduits.

In this study, we investigated the surface characteristics of Chi conduits coated with PDA (Chi/PDA). The mimetic peptides RGI and KLT were loaded onto the Chi/PDA conduits (Chi/PDA-Ps conduits). Next, we investigated the release efficiency of the mimetic peptides from Chi/PDA-Ps conduits. We studied the effects of sustained release of RGI and KLT on Schwann cells (SCs) and human umbilical vein endothelial cells (HUVECs) *in vitro*. Finally, the conduits were implanted into rats with 2 mm sciatic nerve defects. The repair performance of these embedded conduits was evaluated in terms of functional recovery and histological effects.

Materials and Methods

Fabrication of the Chi conduits
The Chi conduits were fabricated as described previously (Li et al., 2021). Briefly, 2% glacial acetic acid (MilliporeSigma, Burlington, MA, USA) was used to dissolve chitosan powder (MilliporeSigma). Molds 1.5 mm in diameter were immersed in the chitosan solution to create the conduits. The molds were removed and the semi-finished conduits were left at room temperature for 1 hour. The chitosan solution in the molds was solidified with 5% sodium hydroxide solution and acetylated with acetic anhydride for 30 minutes. After the reaction, the Chi conduits were stored in 75% ethanol. The conduits used in this study were 1.5 mm in diameter and 6 mm in length.

Chi conduits modified by polydopamine
Dopamine (MilliporeSigma) was dissolved in 10 mM Tris buffer, pH 8.5, to create a 2 mg/mL PDA solution. Once the PDA solution had turned brownish-black, Chi conduits were immersed in the PDA solution for 18 hours. The PDA-coated conduits were then washed with distilled water using an ultrasonic cleaner (SY-360, Jinli, Shanghai, China) until the water became clear to remove the unattached PDA molecules. The conduits were then dried at room temperature.

Surface characterization of chitin conduits and polydopamine-modified chitin conduits
Scanning electron microscope
A field emission scanning electron microscope (JSM-7900F, JEOL Ltd., Tokyo, Japan) was used to observe the surface of Chi and Chi/PDA conduits.

Fourier transform infrared spectrometer analysis
A fourier transform infrared spectrometer (Nicolet 6700, Thermo Fisher Scientific, Waltham, MA, USA) was used to analyze the surface chemical characteristics of Chi and Chi/PDA. The infrared spectra were recorded from 600 to 4000 cm^{-1} with a resolution of 4 cm^{-1}.

Water contact angle measurement
A water contact angle measurement platform (OCA 25, DataPhysics Instruments GmbH, Filderstadt, Germany) was used to evaluate the effect of PDA coating on the Chi surface. The contact angle was measured by the angle formed by the water droplets ($n = 3$) on the surface of the conduits and the conduits.

Immobilization, observation, and release kinetics of mimetic peptides from Chi/PDA-Ps conduits
To display the binding performances of functional peptides to the various conduits, fluorescein isothiocyanate isomer (FITC) RGI (FITC-RGI) and carboxytetramethylrhodamine (TAMRA) KLT (TAMRA-KLT), as well as RGI and KLT alone, were custom synthesized by Shanghai Apeptide Co., Ltd., Shanghai, China. Briefly, each of the peptide powders was dissolved in ultrapure water to 20 µM and sterilized using a 0.22 µm membrane (MilliporeSigma). The prepared peptide solutions were combined 1:1 (v/v) to form RGI/KLT and FITC-RGI/TAMRA-KLT. Sterilized Chi/PDA conduits were placed in a 24-well culture plate with 500 µL of mimetic peptides or fluorescently labeled mimetic peptides for 24 hours to load the peptides.

To visualize the conduits, Chi/PDA-Ps were washed with ultrapure water three times and then viewed under a fluorescence microscope (Leica, Wetzlar, Germany).

For the sustained-release experiment, Chi/PDA conduits loaded with RGI or KLT were immersed in 1 mL phosphate buffered saline (PBS; Beijing Solarbio Science & Technology Co., Ltd., Beijing, China) and gently stirred at 37°C. At each time point, 200 µL of PBS was removed for analysis and was replaced by adding an equal amount of fresh PBS to the conduits. The concentrations of the release samples were determined using a NanoDrop 2000 (Thermo Fisher Scientific).

Isolation and culture of primary Schwann cells and human umbilical vein endothelial cells
Primary SCs were extracted from the sciatic nerves of specific-pathogen-free Sprague-Dawley rats (Beijing Vital River Laboratory Animal Technology Co. Ltd., Beijing, China; license No. SCXK (Jing) 2016-0006) within 72 hours after birth. Ketamine (80 mg/kg, Zhong Mu Bei Kang Pharmaceutical Co., Ltd., Taizhou, China) and xylazine (10 mg/kg, Hua Mu Animal Health Products Inc., Changchun, China) were used to anesthetize rats by intraperitoneal injection. Subsequently, the rats were decapitated with sharp scissors. The epineurium

of the sciatic nerves was peeled off and cut into 1 mm segments. The nerve segments were digested in 2 mg/mL collagenase type I (MilliporeSigma) at 37°C for 15 minutes. The precipitate was collected after centrifugation and resuspended in Dulbecco's Modified Eagle medium/F-12 (Thermo Fisher Scientific) containing 10% fetal bovine serum (Thermo Fisher Scientific). Twenty-four hours later, 1 mM cytarabine (MilliporeSigma) was used to eliminate fibroblasts. The purified SCs were then cultured in a 37°C incubator (Thermo Fisher Scientific) in a 5% CO_2 atmosphere.

HUVECs were purchased from the American Type Culture Collection (Manassas, VA, USA) and cultured in Dulbecco's Modified Eagle medium (Thermo Fisher Scientific) containing 10% fetal bovine serum (Thermo Fisher Scientific) and 1% penicillin/streptomycin solution (Beijing Solarbio Science & Technology Co., Ltd.).

Live/dead staining
Because it is difficult to directly verify the biocompatibility of the surface of conduits, we seeded SCs on Chi, Chi/PDA, or Chi/PDA-Ps films and used the fluorescent live/dead staining kit (Beijing Solarbio Science & Technology Co. Ltd.) to evaluate the biocompatibility of the films. After 3 days, the SCs in each group were washed with PBS three times, the cells were stained with calcein-AM (a green fluorescent dye for live cells) and propidium iodide (a red fluorescent dye for dead cells) for 15 minutes at 37°C, and live and dead cells were observed in 6-well plates by fluorescence microscopy (Leica).

Cellular immunofluorescence
SCs and HUVECs were seeded in 6-well plates at a density of 3×10^5 cells per well. One Chi, Chi/PDA, or Chi/PDA-Ps conduit was placed into each well, and the cells were cultured for 5 days. The SCs and HUVECs were then gently rinsed with 37°C PBS and fixed with 4% paraformaldehyde for 15 minutes. The cell samples were permeabilized with 0.5% Triton X-100 (MilliporeSigma) at room temperature for 5 minutes. The SCs samples were incubated with rabbit anti-S100 antibody (1:400, MilliporeSigma, Cat# S2644, RRID: AB_477501) at 4°C overnight, and the HUVECs samples were incubated with fluorescein phalloidin (1:1000, MilliporeSigma) at room temperature for 1 hour. Alexa Fluor 594-conjugated goat anti-rabbit secondary antibodies (1:200, Abcam, Cambridge, UK, Cat# ab150080, RRID: AB_2650602) were incubated with the SC samples in the dark for 2 hours at room temperature. The samples were gently washed in PBS and incubated with 4',6-diamidino-2-phenylindole dihydrochloride (1:1000, MilliporeSigma) at room temperature for 30 minutes. Finally, a fluorescence microscope (Leica) was used to image the cell samples.

Cell proliferation
SCs and HUVECs were seeded in 12-well plates at a density of 2×10^5 cells per well, and the Chi, Chi/PDA, or Chi/PDA-Ps conduits were added for 1 or 5 days. Then, the cells were incubated with the relevant solution from the Cell Counting Kit-8 (Dojindo Laboratories, Kumamoto, Japan) at 37°C for 2 hours. The absorbance of the medium at 450 nm was read using a microplate reader (Bio-Rad Laboratories).

Enzyme-linked immunosorbent assay
SC secretion ability was assessed by enzyme-linked immunosorbent assay. Briefly, the supernatants of each SC group were collected at 1 and 5 days after the conduit treatment. Enzyme-linked immunosorbent assay kits (Jiangsu Meimian Industrial Co., Yancheng, China) were used in accordance with the manufacturer's instructions to evaluate the levels of BDNF, ciliary neurotrophic factor (CNTF), nerve growth factor (NGF), and VEGF in the supernatants. The absorbance at 450 nm was measured using a microplate reader (Bio-Rad Laboratories, Hercules, CA, USA), and each sample was measured three times.

Human umbilical vein endothelial cell migration assay
HUVECs were seeded in 12-well plates at a density of 2×10^5 cells per well (three replicates per group) and incubated until they reached confluence. A sterile 100 µL tip was used to create a scratch across the surface of each cell layer. Then, the cell layers were washed with PBS to remove detached cells. Chi, Chi/PDA, or Chi/PDA-Ps conduits were placed on the bottom of each well. HUVECs were cultured in Dulbecco's Modified Eagle medium (Thermo Fisher Scientific) containing 2% fetal bovine serum (Thermo Fisher Scientific) for 24 hours and then observed and photographed using an optical microscope (Leica). The rate of wound closure was calculated as follows: Rate of wound closure (%) = $(M_0 - M_{24})/M_0 \times 100$, where M_0 represents the area of the initial wound, and M_{24} represents the area of the wound 24 hours postwounding.

Surgical procedures and conduit implantation
Animal experiments were performed in accordance with the ethical principles of the Institutional Animal Care and Use Committee of the Peking University People's Hospital, Beijing, China (approval No. 2020PHE079; December 10, 2020). All experiments were designed and reported according to the Animal Research: Reporting of *In Vivo* Experiments (ARRIVE) guidelines (Percie du Sert et al., 2020). After PNI, there were sex-related differences in collateral sprouting of axons and pain sensitivity (Kovacic et al., 2003; Stephens et al., 2019). In addition, because female rats are less aggressive than male rats, we chose to use female rats as our experimental animals to eliminate sex-related differences as much as possible. Twenty-four specific-pathogen-free female Sprague-Dawley rats (weighing 200–220 g and aged 6–8 weeks) were supplied by Beijing Vital River Laboratory Animal Technology Co. Ltd. (license No. SCXK (Jing) 2016-0006). The rats were kept in a specific-pathogen-free laboratory at

24 ± 0.5°C and 55 ± 5% humidity with a 12-hour light-dark cycle. All rats were randomly divided into three equal groups according to the implants tested. Before surgery, the animals were anesthetized by inhalation of 3% isoflurane (RWD Life Science Co. Ltd., Shenzhen, China). After shaving the fur at the surgical site, the surgical area was disinfected with iodophor, and the sciatic nerves of the right hind limb in each animal were exposed and cut. The Chi, Chi/PDA, or Chi/PDA-Ps conduits were transplanted using 10-0 nylon sutures under microscope (Leica) guidance to bridge the 2 mm gap between the nerve stumps. After hemostasis and disinfection, the surgical site muscles and skin were sutured in layers. All rats were given unlimited access to food and water after the operation.

Behavioral analysis
We analyzed the recovery of motor function 12 weeks after surgery using walking tracks recorded by the CatWalk XT 10.6 gait analysis system (Noldus, Wageningen, the Netherlands). Briefly, a high-speed camera (Noldus) automatically recorded the rats' paw prints as they crossed a walkway with an illuminated glass floor. Outcome measurements included the paw print area, paw intensity, and the sciatic functional index (SFI). The SFI was measured using the following formula (Rao et al., 2020):

$$SFI = \frac{109.5(ETS-NTS)}{NTS} - \frac{38.3(EPL-NPL)}{NPL} + \frac{13.3(EIT-NIT)}{NIT} - 8.8$$

An SFI of 0 represents normal nerve function, whereas an SFI of −100 represents total nerve dysfunction. ETS indicates the experimental toe spread (the distance from the first to the fifth toe), NTS indicates the normal toe spread, EPL indicates the experimental paw length (distance from the heel to the top of the third toe), NPL indicates the normal paw length, EIT indicates the experimental intermediary toe spread (the distance from the second to the fourth toe), and NIT indicates the normal intermediary toe spread.

Electrophysiological examination
At 12 weeks after surgery, all rats were anesthetized by 3% isoflurane inhalation (RWD Life Science Co., Ltd.), and their right sciatic nerves were exposed. One stimulating electrode was connected 5 mm from the proximal end of the implanted nerve conduit, and we applied an electrical signal with a rectangular pulse (stimulus intensity 0.9 mA, pulse duration 0.1 ms). The latency and amplitude of the compound muscle action potential (CMAP) were recorded for the targeted gastrocnemius muscle with an electrophysiological instrument (Oxford Instruments, Oxford, UK).

Gastrocnemius muscle wet weight analysis
At 12 weeks after surgery, the rats were euthanized by carbon dioxide inhalation with a filling rate of 30–70% per minute. Then, the gastrocnemius muscles of both hind limbs were surgically removed and immediately weighed with an electronic balance (Mettler Toledo, Greifensee, Switzerland). The gastrocnemius muscle wet weight rate was calculated using the following equation: $\text{Wet weight rate} = \frac{w}{W} \times 100\%$, where w indicates the wet weight of the operated muscle, and W indicates the wet weight of the nonoperated muscle.

Tissue analysis
The gastrocnemius muscle specimens were fixed with 4% paraformaldehyde at 4°C overnight. Then the gastrocnemius muscle belly was collected. After dehydration through a graded ethanol series, the specimens were embedded in paraffin and sliced into 5 μm thick cross-sections. For Masson's trichrome staining, the muscle samples were deparaffinized and hydrated. The samples were then placed in Weigert's hematoxylin for 5 minutes to stain cell nuclei, and the samples were rinsed with distilled water. The specimens were then stained with Mayer's hematoxylin, acid ponceau (Beijing Solarbio Science & Technology Co., Ltd.), and aniline blue, in turn, in accordance with the manufacturer's instructions for the Masson's trichrome stain kit (Beijing Solarbio Science & Technology Co., Ltd.). The specimens were dehydrated with 95% ethanol and anhydrous ethanol and observed under a light microscope (Leica). The area and diameter of the gastrocnemius muscle fibers were quantified with ImageJ 1.51j8 (National Institutes of Health, Bethesda, MD, USA) (Schneider et al., 2012).

At 12 weeks after surgery, the sciatic nerves at the surgical sites were collected from all groups (n = 5 rats in each group). The nerve tissues were extracted up to 3 mm from the distal ends of the implanted conduits. The nerve specimens were fixed with 2.5% glutaraldehyde (MilliporeSigma), rinsed, and stained with 1% osmic acid in PBS for 2 hours. The specimens were dehydrated in a series of graded ethanol solutions and then embedded in epoxy resin. An ultramicrotome (Leica) was used to cut the samples into 700 nm thick or 70 nm thick sections. Then, the 700 nm semithin sections were stained with 1% toluidine blue and photographed using a microscope (Olympus Corporation, Tokyo, Japan). For each specimen, photographs were taken from three random fields, and the density of regenerated axons was analyzed. The 70 nm thick ultrathin sections were stained with lead citrate and uranyl acetate and observed under a transmission electron microscope (Philips, Amsterdam, the Netherlands). The thicknesses of the regenerated myelin sheaths and the diameters of the regenerated axons in the indicated areas were recorded and analyzed by ImageJ 1.51j8 (Schneider et al., 2012).

Statistical analysis
No statistical methods were used to predetermine sample sizes; however, our sample sizes were similar to those reported in previous publications (Zhang et al., 2015; Lu et al., 2021). No animals or data points were excluded from the analyses. The evaluator was blinded to the groupings. All numerical data were analyzed using GraphPad Prism, Version 7.04 (GraphPad Software, San Diego, CA, USA, www.graphpad.com) with mean ± standard error of mean (SEM). Student's t-test was used to compare the differences of the water contact angle measurements. Differences among multiple groups were analyzed by one-way analysis of variance followed by Tukey's *post hoc* test. In all analyses, the statistical significance was $P < 0.05$.

Results

Surface characterization of chitin conduits and polydopamine-modified chitin conduits
The Chi conduit was nearly completely transparent, but the Chi/PDA conduit had low transparency and appeared black (**Figure 1A** and **B**). The scanning electron microscope images of the microstructures of the two conduits showed that there were a large number of uniformly distributed PDA particles on the surface of Chi/PDA conduits (**Figure 1C** and **D**).

Fourier transform infrared spectrometer spectra of the Chi and Chi/PDA conduits are shown in **Figure 1E**. Both Chi and Chi/PDA conduits had a broad spectrum corresponding to the -OH group at 3000–3500 cm^{-1}. The Chi/PDA conduits had different -OH and -NH stretching vibrations between 3400–2800 cm^{-1} due to inter- or intramolecular bonds between Chi and PDA. The Chi/PDA conduits had C=O bonds at 1600 cm^{-1} and C=C bonds at 1500 cm^{-1}. These data suggest that PDA particles had been deposited on the Chi surface.

The water contact angles were used to examine the wettability of the Chi and Chi/PDA surfaces. As shown in **Figure 1F–H**, the water contact angle of the Chi surface was approximately 72.4 ± 2.3°, while the angle of the Chi/PDA surface was 5.7 ± 1.4°. PDA greatly reduced the water contact angle of the Chi conduits ($P < 0.01$).

Loading and release efficiencies of mimetic peptides for the Chi/PDA-Ps conduits
Fluorescence imaging and a microplate reader were used to confirm the loading and release of mimetic peptides for the Chi/PDA-Ps conduits (**Figure 2A**). Fluorescent activation of FITC (green) and TAMRA (orange) suggested that FITC-RGI and TAMRA-KLT were immobilized on the surface of the Chi/PDA conduits (**Figure 2B**). There was no significant fluorescence in Chi/PDA conduits (image not shown).

The release curves of RGI and KLT release from Chi/PDA conduits at 37°C in PBS are shown in **Figure 2C**. The release curves of RGI and KLT had an upward trend for the first 8 days. The release of KLT was greater than that of RGI from the 4th to the 9th day, but the peak of RGI release did not appear until the 12th day. The different release rates might be related to the unequal molecular weights and different chemical and structural natures of the two functional peptides.

Cytotoxicity of Chi/PDA-Ps conduits
As shown in **Figure 3A**, the SCs were seeded on films with Chi, Chi/PDA, or Chi/PDA-Ps. After live/dead staining, the live cells appeared green by calcein-AM staining, and the dead cells were stained red by propidium iodide (**Figure 3B**). There were fewer live cells and more dead cells in the Chi group than in the other two groups. There was no obvious difference in live and dead cell numbers between the Chi/PDA and Chi/PDA-Ps groups. There was a greater proportion of live cells in the PDA-modified groups than in the Chi group (**Figure 3C**). This experiment showed that both the pure Chi substrate and the PDA-modified substrates were not cytotoxic *in vitro*, and the PDA-modified substrates were more biocompatible than the Chi substrate.

Chi/PDA-Ps conduits enhance Schwann cells proliferation and levels of secreted neurotrophic factors *in vitro*
SCs were treated with Chi, Chi/PDA, or Chi/PDA-Ps conduits for 5 days to evaluate functional alterations. On the 5th day, immunofluorescence results showed that the SCs were fusiform or polygonal in shape, indicating that the cells were healthy. The number of SCs in the Chi/PDA-Ps group was significantly higher than that in the Chi and Chi/PDA groups (**Figure 4A**). Moreover, after 1 day of treatment, there was no difference in the proliferation ability among the three groups of SCs ($P > 0.05$). After 5 days of treatment, the proliferation ability of SCs in the Chi/PDA-Ps group was significantly greater than that in the other groups ($P < 0.05$; **Figure 4B**). The levels of the neurotrophic factors CNTF, BDNF, NGF, and VEGF that were released from SCs into the culture medium were determined by enzyme-linked immunosorbent assay. In **Figure 4C–F**, it was found that CNTF, BDNF, NGF, and VEGF were released from SCs at higher levels at 1 and 5 days after Chi/PDA-Ps conduits treatment compared with Chi and Chi/PDA treatment.

Chi/PDA-Ps conduits promote attachment, proliferation, and migration of HUVECs *in vitro*
The HUVECs stained positive for a vascular endothelial cell marker, CD31 (**Additional file 1**). As shown in **Figure 5A**, HUVECs exhibited a more extended spreading of the cytoskeleton after treatment with Chi/PDA-Ps. A HUVEC proliferation assay was used to evaluate the proangiogenic effects of the functional peptides released from Chi/PDA-Ps conduits. The results showed that Chi/PDA-Ps conduits could greatly improve the HUVEC proliferation on the 5th day (**Figure 5B**). A scratch test was performed to assess cell migration (**Figure 5C** and **D**). After 24 hours of incubation, HUVECs treated with RGI and KLT migrated the most among the three groups, covering more than 77.1% of the initial wounded area. The rate of wound closure was greater in the Chi/PDA group than in the Chi group.

Chi/PDA-Ps conduits improve sciatic nerve function and reduces gastrocnemius atrophy in rats with sciatic nerve injury

The three-dimensional pressure diagram of paw prints of each group presented that the spread of each toe and the toe pressure of the right foot in the Chi/PDA-Ps group were greater than those in the Chi and Chi/PDA groups (**Figure 6A**). The SFI of the Chi/PDA group was higher than the Chi group ($P < 0.01$). In addition, the SFI was significantly improved in the Chi/PDA-Ps group compared with that in the Chi group ($P < 0.01$) and Chi/PDA group ($P < 0.01$) (**Figure 6B**).

The degree of gastrocnemius muscle atrophy induced by PNI was evaluated by the wet weight rate. As shown in **Figure 6C**, Chi/PDA-Ps treatment inhibited gastrocnemius muscle atrophy more than Chi and Chi/PDA conduit treatment.

Masson's trichrome staining of the cross-sectional area of the gastrocnemius muscles showed no obvious fibrosis or inflammatory cell infiltration in the gastrocnemius muscles among the three treatment groups (**Figure 6D**). The mean value of the cross-sectional areas of the muscle fibers was highest in the Chi/PDA-Ps group and lowest in the Chi group (**Figure 6E**).

Chi/PDA-Ps conduits improve the recovery of electrical conduction of nerves in rats with sciatic nerve injury

Electrophysiology experiments examined the recovery of electrical conduction of nerves. The representative CMAP images in each group are shown in **Figure 7A**. The quantitations of CMAP latency and amplitude are shown in **Figure 7B** and **C**. There was no significant difference in proximal CMAP latency between the Chi and Chi/PDA groups ($P > 0.05$), but proximal CMAP latency was longer in the Chi and Chi/PDA groups than in the Chi/PDA-Ps group ($P < 0.05$). In addition, the amplitude of CMAP was significantly higher in the Chi/PDA-Ps group than in the Chi and Chi/PDA groups ($P < 0.05$).

Chi/PDA-Ps conduits improve axonal regeneration and remyelination in rats with sciatic nerve injury

At 12 weeks after surgery, the regenerated sciatic nerve was exposed and evaluated. We observed that new connections had formed at both ends of the nerve defect. The gross morphology of nerves treated with Chi, Chi/PDA, or Chi/PDA-Ps showed no neuroma formation at the suture site in all groups, and there was no apparent inflammation or tissue adhesion around the conduits (**Figure 8A**).

To evaluate the neuroregenerative effect of mimetic peptide-loaded conduits *in vivo*, we isolated the regenerated sciatic nerves of all rats. According to toluidine blue staining (**Figure 8B**), the number of regenerated nerves was greater in the Chi/PDA-Ps group than in the Chi and Chi/PDA groups ($P < 0.05$). The results of transmission electron microscopy revealed that the diameters of regenerated nerve fibers and the thicknesses of myelin sheaths were greatest in the Chi/PDA-Ps group ($P < 0.05$). However, there were no significant differences in the diameters of regenerated nerve fibers or the thicknesses of myelin sheaths between the Chi/PDA and Chi groups ($P > 0.05$; **Figure 8C–F**).

Discussion

Inspired by the nerve-selective regeneration theory, our team has confirmed that repair of PNI is improved by the application of small gap tubulization technology (Zhang et al., 2015, 2018). The small gap formed between the conduit and the nerve stumps can reduce nerve tension, provide a stable microenvironment for axon regeneration, improve the accuracy of nerve fiber anastomosis, and protect the injured nerve during healing (Zhang et al., 2021). Chi has been used widely in tissue engineering because of its antibacterial activity, biocompatibility, nontoxicity, and biodegradability (Lu et al., 2021). Additionally, it is important to supplement Chi conduits with growth-accelerating and neural cell-regulating cytokines to better accelerate nerve regeneration.

Recently, numerous advantages and unique properties of PDA have increased its use in various biology and biomaterials disciplines (Liu et al., 2014). In the present study, we took advantage of the spontaneous polymerization of PDA to modify Chi conduits without requiring specialized equipment or procedures or harsh reaction conditions. The results of transmission electron microscopy and Fourier transform infrared spectrometry confirmed that PDA was successfully coated on the surface of Chi conduits. PDA coverage reduced the water contact angle of the Chi surface, increasing biocompatibility (Zhao et al., 2005), which may explain the difference we observed in live/dead staining between Chi-treated SCs and the other SCs modified by PDA. By calculating the amount of mimetic peptide, we estimated the total quantities of RGI and KLT released from Chi/PDA-Ps conduits were 3.10 ± 0.05 μmol and 2.66 ± 0.03 μmol, respectively. As a result, the functional peptides loaded onto Chi/PDA substrates appear to be in a sustained-release state.

BDNF is one of the most essential neurotrophic factors, and it plays a critical role in the growth and differentiation of new neurons, the maintenance of axons, and the survival of neurons after PNI (Benarroch, 2015; Bierlein De la Rosa et al., 2017). The concentration of exogenous BDNF is closely related to axon regeneration. Richner et al. (2014) reported that excessively high doses of BDNF inhibited the regeneration of neuronal axons. In addition, VEGF is an influential angiogenic factor with a major function of increasing vascular permeability and promoting endothelial cell survival, proliferation, and

migration (Verheyen et al., 2013). Moreover, increased expression of VEGF leads to enhanced neurite outgrowth and neuron survival, which leads to neurotrophic and neuroprotective effects (Guaiquil et al., 2014; Lange et al., 2016). BDNF promotes vascular endothelial cell survival and vessel stability (He et al., 2018). However, the delivery of multiple growth factors to an injury site has disadvantages, such as high cost, rapid degradation, the impracticality of regular injection requirements, and unexpected adverse effects (Lee et al., 2011; Wang et al., 2017b). Thus, we chose BDNF and VEGF mimetic peptides that have established synthesis methods and well-documented functions to be loaded on Chi conduits. We previously developed an aligned chitosan nanofiber hydrogel grafted with RGI and KLT and demonstrated that it promoted nerve regeneration (Rao et al., 2020). However, hydrogel's large volume and slow degradation make it unsuitable for filling small 2 mm nerve defects. Here, we took advantage of the excellent adhesion properties of PDA to construct peripheral nerve conduits that allowed sufficient nerve regeneration space and sustained release of functional peptides.

The peripheral nervous system is able to regenerate. This ability is largely due to SCs, which can support axon regeneration and remyelination (Nocera and Jacob, 2020). During the early stage of nerve regeneration, SCs quickly proliferate to remove myelin fragments. In the later stage of regeneration, SCs adopt an elongated, bipolar morphology to form regeneration tracks, named Büngner bands, that guide axon regeneration to the distal site (Jessen et al., 2015; Jessen and Mirsky, 2016). SCs also upregulate expression of neurotrophic factors such as BDNF, NGF, CNTF, and VEGF. These favorable regeneration factors promote the survival of injured neurons and the outgrowth of axons (Fontana et al., 2012; Brushart et al., 2013). In the current study, the Chi/PDA-Ps conduits promoted SC proliferation and secretion of neurotrophic factors from SCs *in vitro*.

The vascular system is essential for the development and regeneration of peripheral nerve tissue (Wang et al., 2017a). Newly formed blood vessels act as paths that induce SC migration, which in turn, induces axon elongation (Cattin et al., 2015). In addition to the blood vessels in the epineurium, there are also rich vascular networks between the perineurium and the endoneurium that continuously provide oxygen and nutrition to neural cells. An ischemic and hypoxic environment caused by disrupted blood circulation at the injured site delays peripheral nerve regeneration (Wang et al., 2013). Insufficient blood circulation can lead to degeneration and necrosis of surrounding tissues, which limits the therapeutic effect of transplanted nerve conduits. It has been shown that the exposure of nerve scaffolds to hypoxic conditions leads to necrosis of neural cells and seed cells and greatly affects peripheral nerve regeneration (Khademhosseini et al., 2006; Ma et al., 2020). Therefore, the coordinated relationship between multiple systems, especially the vascular system, should be considered when conducting peripheral nerve regeneration research. In the present study, we designed nerve conduits that effectively promoted the proliferation and migration of HUVECs.

Walking reflects the coordination between sensory inputs, cortical integration, and motor responses. Gait analysis is an objective indicator that reflects the degree of sciatic nerve recovery (Varejão et al., 2001), and SFI is an objective indicator that is used to quantify sciatic nerve recovery. Our SFI results demonstrated that improved motor function recovery was achieved after treatment with the RGI and KLT functional peptides. Electrophysiological analysis showed that Chi/PDA-Ps conduits improved the recovery of sciatic nerve conduction function. We also quantified a greater number of nerve fibers and a larger diameter of myelinated nerve fibers in the Chi/PDA-Ps group compared with those in the Chi and Chi/PDA groups. These findings indicate that functional peptide-based sustained-release conduits were effective in enhancing peripheral nerve regeneration and improving nerve function recovery. However, the optimal concentration and sustained-release patterns of mimetic peptides used in peripheral nerve regeneration require further study.

In this study, we prepared a Chi nerve conduit using PDA as a peptide carrier. Our *in vitro* studies indicate that Chi/PDA-Ps conduits successfully supplied functional activators to promote the proliferation of SCs and endothelial cells. In addition, the secretion of neurotrophic factors from SCs and the migration of endothelial cells were improved by sustained release of the RGI and KLT mimetic peptides. *In vivo* analysis revealed that the PNI rats treated with Chi/PDA-Ps conduits had improved axonal regeneration, remyelination, and functional recovery. Our research is expected to provide a practical experimental and theoretical basis for further improvement of peripheral nerve conduit design and use.
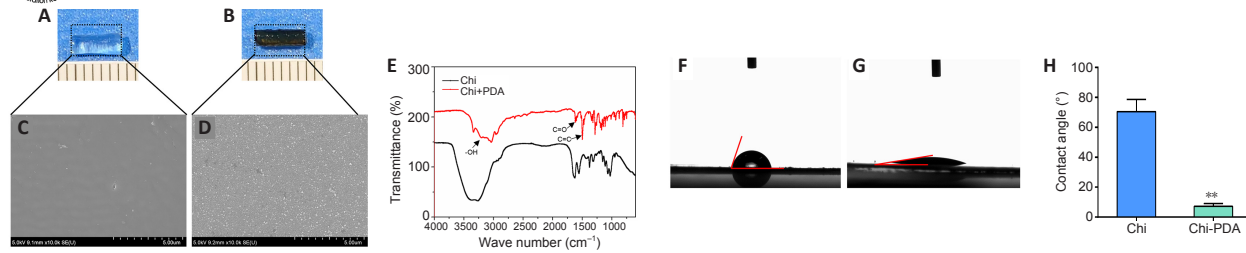
Figure 1 | Chitin (Chi) surface properties after polydopamine (PDA) modification.
(A, B) Visualization of the Chi conduits without (A) or with (B) PDA under general observation. The Chi conduit was nearly transparent, while the Chi/PDA conduit appeared black with low transparency. Scale bars: 1 mm. (C, D) Microstructure by scanning electron microscope of Chi surface without (C) or with (D) PDA. There were a large number of uniformly distributed PDA particles on the surface of Chi/PDA conduits. Scale bars: 5 μm. (E) Element composition of Chi and Chi/PDA surfaces were evaluated by Fourier transform infrared spectrometer spectra. Arrows indicate characteristic peaks. (F, G) Water drops on Chi (F) and Chi/PDA (G) surfaces. PDA greatly reduced the water contact angle of the Chi conduits. (H) Quantitative results of water contact angles for the Chi and Chi/PDA surfaces. Data are expressed as the mean ± SEM. The experiments were repeated three times. **$P < 0.01$, *vs.* Chi group (Student's *t*-test). Chi: Chitin; Chi/PDA: polydopamine-coated chitin conduits.
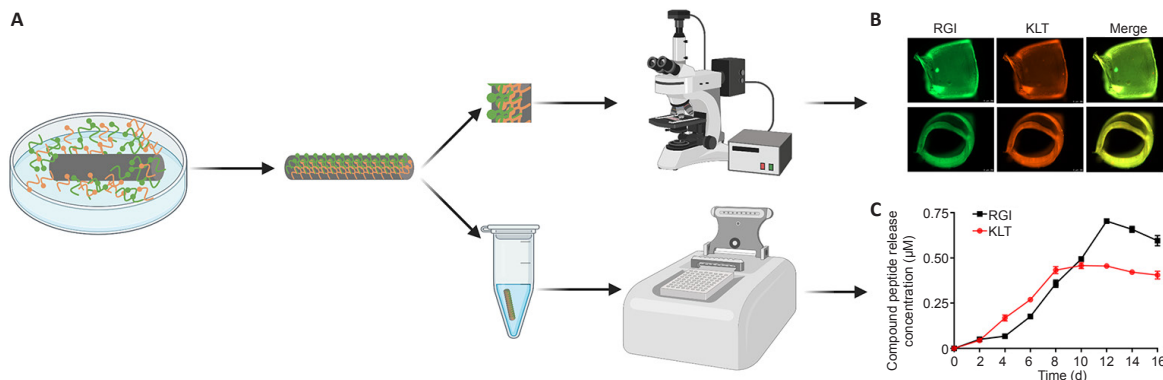

Figure 2 | Observation and release kinetics of mimetic peptides from Chi/PDA-Ps conduits.
(A) Schematic diagram of Chi/PDA-Ps conduit preparation. (B) Side and cross-section view after functional peptides were immobilized on Chi/PDA conduits. RGI was modified with FITC (green fluorescence) and KLT was modified with TAMRA (orange fluorescence). (C) Release curves of RGI and KLT from Chi/PDA-Ps conduits. Data are expressed as mean ± SEM. The experiments were repeated three times. Chi/PDA: Polydopamine-coated chitin conduits; Chi/PDA-Ps: polydopamine-coated chitin conduits loaded with functional peptides; FITC: fluorescein isothiocyanate isomer; RGI: RGIDKRHWNSQ; KLT: KLTWQELYQLKYKGI; TAMRA: carboxytetramethylrhodamine.
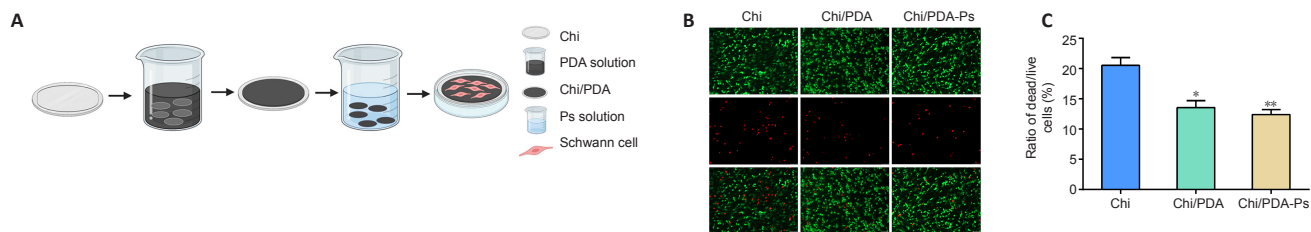

Figure 3 | Cytotoxicity of Chi/PDA-Ps conduits.
(A) Schematic representation of SCs seeded onto Chi/PDA-Ps films. (B) The survival ability of SCs seeded on different films and analyzed with a live/dead staining kit. The number of live cells (green, calcein-AM) was lower in the Chi group than in the other two groups, and the number of dead cells (red, propidium iodide) was greater in the Chi group than in the other two groups. Scale bars: 50 μm. (C) Quantitative results of the percent of dead/live cells. All data are represented as the mean ± SEM ($n = 3$ for each group). *$P < 0.05$, **$P < 0.01$, *vs.* Chi group (one-way analysis of variance followed by Tukey's *post hoc* test). Chi: Chitin; Chi/PDA: polydopamine-coated chitin conduits; Chi/PDA-Ps: polydopamine-coated chitin conduits loaded with functional peptides; SCs: Schwann cells.
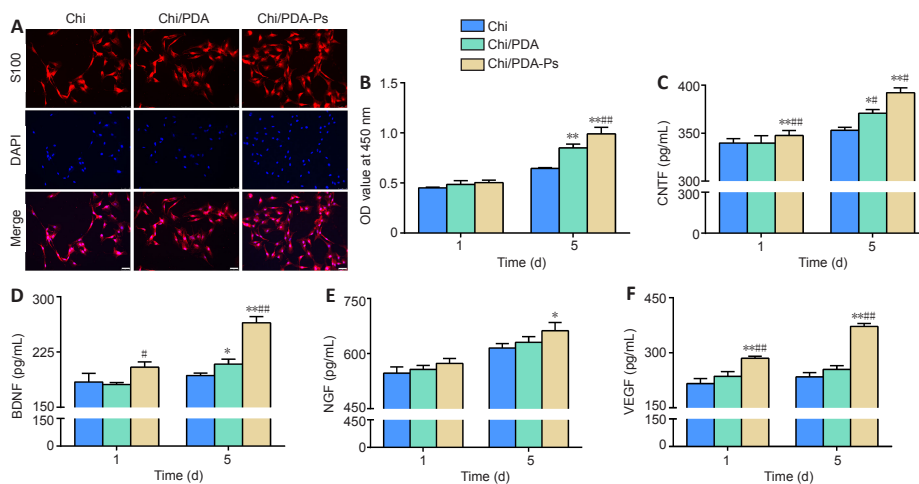

Figure 4 | Chi/PDA-Ps conduits promote SCs proliferation and secretion.
(A) SCs were identified by S100 staining (red, Alexa Fluor 594) and nucleus staining (blue, DAPI). The number of SCs in the Chi/PDA-Ps group was larger than those in the Chi and PDA groups. Scale bars: 50 μm. (B) SCs proliferation analysis was performed using a Cell Counting Kit-8 (Dojindo Laboratories). (C–F) Protein levels of CNTF, BDNF, NGF, and VEGF in supernatant by enzyme-linked immunosorbent assay. All data are represented as the mean ± SEM ($n = 3$ for each group). *$P < 0.05$, **$P < 0.01$, *vs.* Chi group; #$P < 0.05$, ##$P < 0.01$, *vs.* Chi/PDA group (one-way analysis of variance followed by Tukey's *post hoc* test). BDNF: Brain-derived neurotrophic factor; Chi: chitin; Chi/PDA: polydopamine-coated chitin conduits; Chi/PDA-Ps: polydopamine-coated chitin conduits loaded with functional peptides; CNTF: ciliary neurotrophic factor; DAPI: 4′,6-diamidino-2-phenylindole; NGF: nerve growth factor; OD: optical density; SCs: Schwann cells; VEGF: vascular endothelial growth factor.
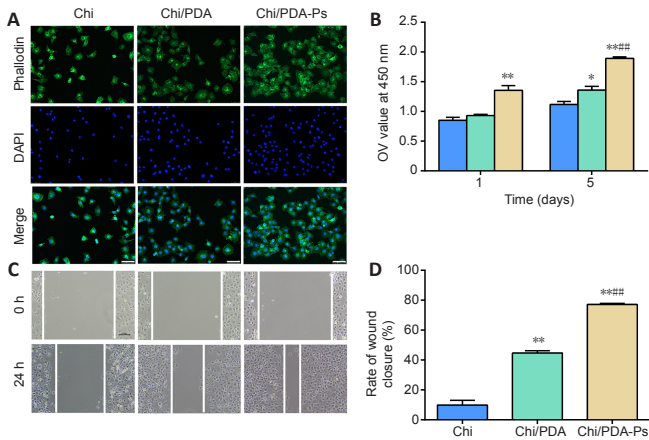
Figure 5 | Chi/PDA-Ps conduits accelerate the attachment, proliferation, and migration of HUVECs.
(A) HUVECs were identified by phalloidin staining (green, FITC) and nucleus staining (blue, DAPI). The HUVECs in the Chi/PDA-Ps group had more extended morphology than those in the other groups. Scale bars: 75 μm. (B) The Cell Counting Kit-8 (Dojindo Laboratories) determined HUVECs proliferation after treatment with the various conduits. (C) A representative photograph of HUVECs migration in the wound healing assay. The migration distance was longer in the Chi/PDA-Ps group than in the other groups. Scale bars: 100 μm. (D) Quantitative results for HUVECs migration in the wound healing assay. All data are represented as the mean ± SEM (n = 3 for each group). *P < 0.05, **P < 0.01, vs. Chi group; ##P < 0.01, vs. Chi/PDA group (one-way analysis of variance followed by Tukey's $post hoc$ test). Chi: Chitin; Chi/PDA: polydopamine-coated chitin conduits; Chi/PDA-Ps: polydopamine-coated chitin conduits loaded with functional peptides; DAPI: 4′,6-diamidino-2-phenylindole; FITC: fluorescein isothiocyanate isomer; HUVECs: human umbilical vein endothelial cells; OD: optical density.
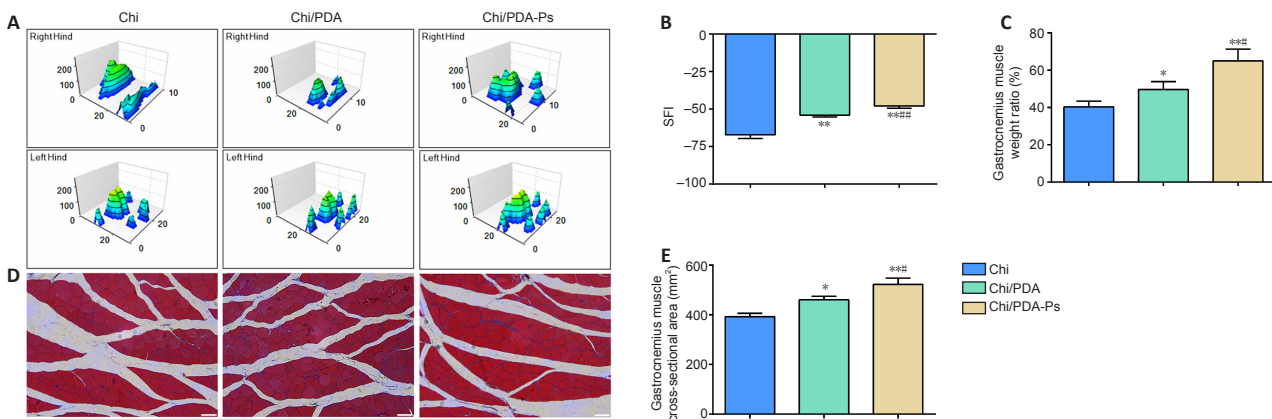

Figure 6 | Chi/PDA-Ps conduits improve motor functional recovery in PNI rats 12 weeks after surgery.
(A) Representative 3D plantar pressure distribution of affected hind limbs and healthy hind limbs for each group. The spread and the toe stress of the right hind limb were greater in the Chi/PDA-Ps group than in the other groups. (B) Quantitative results of the SFI values (n = 3 for each group). (C) Quantitative results of the gastrocnemius muscle wet weight rate (n = 3 for each group). (D) Cross-sectional area of gastrocnemius muscle fibers 12 weeks after surgery. The cross-sectional area of muscle fibers was greater in the Chi/PDA-Ps group than in the other groups. Scale bars: 50 μm. (E) Quantitative results of the cross-section of the gastrocnemius muscle fiber (n = 8 for each group). All data are represented as the mean ± SEM. *P < 0.05, **P < 0.01, vs. Chi group; #P < 0.05, ##P < 0.01, vs. Chi/PDA group (one-way analysis of variance followed by Tukey's $post hoc$ test). 3D: Three-dimensional; Chi: Chitin; Chi/PDA: polydopamine-coated chitin conduits; Chi/PDA-Ps: polydopamine-coated chitin conduits loaded with functional peptides; PNI: peripheral nerve injury; SFI: sciatic functional index.
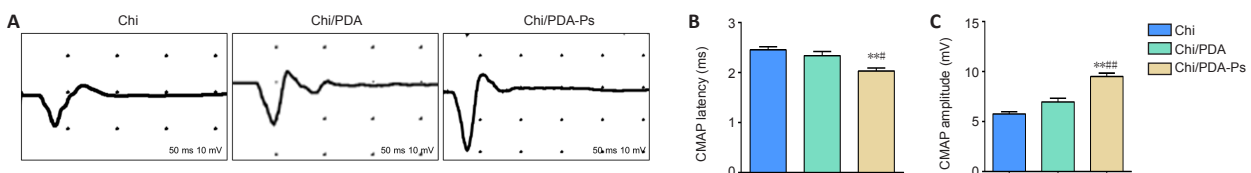

Figure 7 | The continuous release of mimetic peptides from Chi/PDA-Ps conduits enhances conduction function of the regenerated sciatic nerve.
(A) Typical electromyography 12 weeks after surgery. The rats in the Chi/PDA-Ps group had shorter CMAP latency and higher CMAP amplitude than those in the other groups. Abscissa, 50 ms/lattice; ordinate, 10 mV/lattice. (B) The latency of CMAPs 12 weeks after surgery. (C) The amplitude of CMAPs 12 weeks after surgery. All data are represented as the mean ± SEM (n = 8 for each group). **P < 0.01, vs. Chi group; #P < 0.05, ##P < 0.01, vs. Chi/PDA group (one-way analysis of variance followed by Tukey's $post hoc$ test). Chi: Chitin; Chi/PDA: polydopamine-coated chitin conduits; Chi/PDA-Ps: polydopamine-coated chitin conduits loaded with functional peptides; CMAP: compound motor action potential.
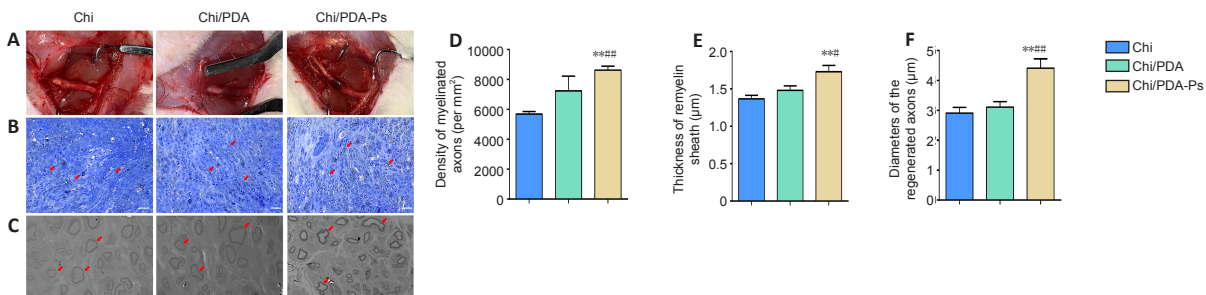

Figure 8 | Chi/PDA-Ps conduits facilitate axonal regeneration and remyelination.
(A) General view of Chi, Chi/PDA, and Chi/PDA-Ps conduits 12 weeks after surgery. We observed no neuroma, inflammation, or tissue adhesion around the conduits. (B) The regenerated nerves were subjected to toluidine blue staining. More nerve axons (red arrows) were observed in the Chi/PDA-Ps group. Scale bars: 50 μm. (C) The regenerated nerves were subjected to transmission electron microscope observation. Regenerated axons with thick myelin sheaths (red arrows) were more common in the Chi/PDA-Ps group. Scale bars: 5 μm. (D) Quantification of the density of myelinated nerve fibers. (E) Quantification of the myelin sheath thickness. (F) Quantification of the diameter of myelinated nerve fibers. All data are represented as the mean ± SEM (n = 8 for each group). **P < 0.01, vs. Chi group; #P < 0.05, ##P < 0.01, vs. Chi/PDA group (one-way analysis of variance followed by Tukey's $post hoc$ test). Chi: Chitin; Chi/PDA: polydopamine-coated chitin conduits; Chi/PDA-Ps: polydopamine-coated chitin conduits loaded with functional peptides.

Open peer reviewer: *Aldo Calliari, Universidad de la República, Uruguay.*
Additional files:
Additional file 1: Identification of human umbilical vein endothelial cells.
Additional file 2: Open peer review report 1.

References

Benarroch EE (2015) Brain-derived neurotrophic factor: Regulation, effects, and potential clinical relevance. Neurology 84:1693-1704.

Bierlein De la Rosa M, Sharma AD, Mallapragada SK, Sakaguchi DS (2017) Transdifferentiation of brain-derived neurotrophic factor (BDNF)-secreting mesenchymal stem cells significantly enhance BDNF secretion and Schwann cell marker proteins. J Biosci Bioeng 124:572-582.

Brushart TM, Aspalter M, Griffin JW, Redett R, Hameed H, Zhou C, Wright M, Vyas A, Höke A (2013) Schwann cell phenotype is regulated by axon modality and central-peripheral location, and persists in vitro. Exp Neurol 247:272-281.

Cattin AL, Burden JJ, Van Emmenis L, Mackenzie FE, Hoving JJ, Garcia Calavia N, Guo Y, McLaughlin M, Rosenberg LH, Quereda V, Jamecna D, Napoli I, Parrinello S, Enver T, Ruhrberg C, Lloyd AC (2015) Macrophage-induced blood vessels guide Schwann cell-mediated regeneration of peripheral nerves. Cell 162:1127-1139.

Cheng W, Zeng X, Chen H, Li Z, Zeng W, Mei L, Zhao Y (2019) Versatile polydopamine platforms: synthesis and promising applications for surface modification and advanced nanomedicine. ACS Nano 13:8537-8565.

D'Andrea LD, Iaccarino G, Fattorusso R, Sorriento D, Carannante C, Capasso D, Trimarco B, Pedone C (2005) Targeting angiogenesis: structural characterization and biological properties of a de novo engineered VEGF mimicking peptide. Proc Natl Acad Sci U S A 102:14215-14220.

Fontana X, Hristova M, Da Costa C, Patodia S, Thei L, Makwana M, Spencer-Dene B, Latouche M, Mirsky R, Jessen KR, Klein R, Raivich G, Behrens A (2012) c-Jun in Schwann cells promotes axonal regeneration and motoneuron survival via paracrine signaling. J Cell Biol 198:127-141.

Guaiquil VH, Pan Z, Karagianni N, Fukuoka S, Alegre G, Rosenblatt MI (2014) VEGF-B selectively regenerates injured peripheral neurons and restores sensory and trophic functions. Proc Natl Acad Sci U S A 111:17272-17277.

He T, Sun R, Li Y, Katusic ZS (2018) Effects of brain-derived neurotrophic factor on MicroRNA expression profile in human endothelial progenitor cells. Cell Transplant 27:1005-1009.

Jacob C (2017) Chromatin-remodeling enzymes in control of Schwann cell development, maintenance and plasticity. Curr Opin Neurobiol 47:24-30.

Jessen KR, Mirsky R (2016) The repair Schwann cell and its function in regenerating nerves. J Physiol 594:3521-3531.

Jessen KR, Arthur-Farraj P (2019) Repair Schwann cell update: adaptive reprogramming, EMT, and stemness in regenerating nerves. Glia 67:421-437.

Jessen KR, Mirsky R, Lloyd AC (2015) Schwann cells: development and role in nerve repair. Cold Spring Harb Perspect Biol 7:a020487.

Jiang B, Liang S, Peng ZR, Cong H, Levy M, Cheng Q, Wang T, Remais JV (2017) Transport and public health in China: the road to a healthy future. Lancet 390:1781-1791.

Khademhosseini A, Langer R, Borenstein J, Vacanti JP (2006) Microscale technologies for tissue engineering and biology. Proc Natl Acad Sci U S A 103:2480-2487.

Kilkenny C, Browne W, Cuthill IC, Emerson M, Altman DG; National Centre for the Replacement, Refinement and Reduction of Amimals in Research (2011) Animal research: reporting in vivo experiments--the ARRIVE guidelines. J Cereb Blood Flow Metab 31:991-993.

Kou Y, Peng J, Wu Z, Yin X, Zhang P, Zhang Y, Weng X, Qiu G, Jiang B (2013) Small gap sleeve bridging can improve the accuracy of peripheral nerve selective regeneration. Artif Cells Nanomed Biotechnol 41:402-407.

Kovacic U, Sketelj J, Bajrović FF (2003) Sex-related difference in collateral sprouting of nociceptive axons after peripheral nerve injury in the rat. Exp Neurol 184:479-488.

Lange C, Storkebaum E, de Almodóvar CR, Dewerchin M, Carmeliet P (2016) Vascular endothelial growth factor: a neurovascular target in neurological diseases. Nat Rev Neurol 12:439-454.

Lee K, Silva EA, Mooney DJ (2011) Growth factor delivery-based tissue engineering: general approaches and a review of recent developments. J R Soc Interface 8:153-170.

Li C, Liu SY, Pi W, Zhang PX (2021) Cortical plasticity and nerve regeneration after peripheral nerve injury. Neural Regen Res 16:1518-1523.

Liu Y, Ai K, Lu L (2014) Polydopamine and its derivative materials: synthesis and promising applications in energy, environmental, and biomedical fields. Chem Rev 114:5057-5115.

Lopes CDF, Gonçalves NP, Gomes CP, Saraiva MJ, Pêgo AP (2017) BDNF gene delivery mediated by neuron-targeted nanoparticles is neuroprotective in peripheral nerve injury. Biomaterials 121:83-96.

Lu C, Wang Y, Yang S, Wang C, Sun X, Lu J, Yin H, Jiang W, Meng H, Rao F, Wang X, Peng J (2018) Bioactive self-assembling peptide hydrogels functionalized with brain-derived neurotrophic factor and nerve growth factor mimicking peptides synergistically promote peripheral nerve regeneration. ACS Biomater Sci Eng 4:2994-3005.

Lu CF, Wang B, Zhang PX, Han S, Pi W, Kou YH, Jiang BG (2021) Combining chitin biological conduits with small autogenous nerves and platelet-rich plasma for the repair of sciatic nerve defects in rats. CNS Neurosci Ther 27:805-819.

Ma T, Yang Y, Quan X, Lu L, Xia B, Gao J, Qi F, Li S, Zhao L, Mei L, Zheng Y, Shen Y, Luo Z, Jin Y, Huang J (2020) Oxygen carrier in core-shell fibers synthesized by coaxial electrospinning enhances Schwann cell survival and nerve regeneration. Theranostics 10:8957-8973.

Nocera G, Jacob C (2020) Mechanisms of Schwann cell plasticity involved in peripheral nerve repair after injury. Cell Mol Life Sci 77:3977-3989.

Percie du Sert N, Hurst V, Ahluwalia A, Alam S, Avey MT, Baker M, Browne WJ, Clark A, Cuthill IC, Dirnagl U, Emerson M, Garner P, Holgate ST, Howells DW, Karp NA, Lazic SE, Lidster K, MacCallum CJ, Macleod M, Pearl EJ, et al. (2020) The ARRIVE guidelines 2.0: Updated guidelines for reporting animal research. PLoS Biol 18:e3000410.

Rao F, Yuan Z, Zhang D, Yu F, Li M, Li D, Jiang B, Wen Y, Zhang P (2019) Small-molecule SB216763-loaded microspheres repair peripheral nerve injury in small gap tubulization. Front Neurosci 13:489.

Rao F, Wang Y, Zhang D, Lu C, Cao Z, Sui J, Wu M, Zhang Y, Pi W, Wang B, Kou Y, Wang X, Zhang P, Jiang B (2020) Aligned chitosan nanofiber hydrogel grafted with peptides mimicking bioactive brain-derived neurotrophic factor and vascular endothelial growth factor repair long-distance sciatic nerve defects in rats. Theranostics 10:1590-1603.

Riaz Rajoka MS, Mehwish HM, Wu Y, Zhao L, Arfat Y, Majeed K, Anwaar S (2020) Chitin/chitosan derivatives and their interactions with microorganisms: a comprehensive review and future perspectives. Crit Rev Biotechnol 40:365-379.

Rubert Pérez CM, Álvarez Z, Chen F, Aytun T, Stupp SI (2017) Mimicking the bioactivity of fibroblast growth factor-2 using supramolecular nanoribbons. ACS Biomater Sci Eng 3:2166-2175.

Stephens KE, Zhou W, Ji Z, Chen Z, He S, Ji H, Guan Y, Taverna SD (2019) Sex differences in gene regulation in the dorsal root ganglion after nerve injury. BMC Genomics 20:147.

Tang P, Han L, Li P, Jia Z, Wang K, Zhang H, Tan H, Guo T, Lu X (2019) Mussel-inspired electroactive and antioxidative scaffolds with incorporation of polydopamine-reduced graphene oxide for enhancing skin wound healing. ACS Appl Mater Interfaces 11:7703-7714.

Varejão AS, Meek MF, Ferreira AJ, Patrício JA, Cabrita AM (2001) Functional evaluation of peripheral nerve regeneration in the rat: walking track analysis. J Neurosci Methods 108:1-9.

Verheyen A, Peeraer E, Lambrechts D, Poesen K, Carmeliet P, Shibuya M, Pintelon I, Timmermans JP, Nuydens R, Meert T (2013) Therapeutic potential of VEGF and VEGF-derived peptide in peripheral neuropathies. Neuroscience 244:77-89.

Wang H, Zhu H, Guo Q, Qian T, Zhang P, Li S, Xue C, Gu X (2017a) Overlapping mechanisms of peripheral nerve regeneration and angiogenesis following sciatic nerve transection. Front Cell Neurosci 11:323.

Wang Y, Qi F, Zhu S, Ye Z, Ma T, Hu X, Huang J, Luo Z (2013) A synthetic oxygen carrier in fibrin matrices promotes sciatic nerve regeneration in rats. Acta Biomater 9:7248-7263.

Wang Z, Wang Z, Lu WW, Zhen W, Yang D, Peng S (2017b) Novel biomaterial strategies for controlled growth factor delivery for biomedical applications. NPG Asia Mater 9:e435-e435.

Xia B, Lv Y (2018) Dual-delivery of VEGF and NGF by emulsion electrospun nanofibrous scaffold for peripheral nerve regeneration. Mater Sci Eng C Mater Biol Appl 82:253-264.

Younes I, Rinaudo M (2015) Chitin and chitosan preparation from marine sources. Structure, properties and applications. Mar Drugs 13:1133-1174.

Zhang M, Li C, Zhou LP, Pi W, Zhang PX (2021) Polymer scaffolds for biomedical applications in peripheral nerve reconstruction. Molecules 26:2712.

Zhang P, Han N, Wang T, Xue F, Kou Y, Wang Y, Yin X, Lu L, Tian G, Gong X, Chen S, Dang Y, Peng J, Jiang B (2013) Biodegradable conduit small gap tubulization for peripheral nerve mutilation: a substitute for traditional epineurial neurorrhaphy. Int J Med Sci 10:171-175.

Zhang PX, Li-Ya A, Kou YH, Yin XF, Xue F, Han N, Wang TB, Jiang BG (2015) Biological conduit small gap sleeve bridging method for peripheral nerve injury: regeneration law of nerve fibers in the conduit. Neural Regen Res 10:71-78.

Zhang PX, Jin F, Li ZL, Wu WL, Li YY, Long JH, Chen GY, Chen XX, Gan JY, Gong XY, He QY, Bi T (2018) A randomized phase II trial of induction chemotherapy followed by cisplatin chronotherapy versus constant rate delivery combined with radiotherapy. Chronobiol Int 35:240-248.

Zhao G, Schwartz Z, Wieland M, Rupp F, Geis-Gerstorfer J, Cochran DL, Boyan BD (2005) High surface energy enhances cell response to titanium substrate microstructure. J Biomed Mater Res A 74:49-58.

C-Editor: Zhao M; S-Editors: Yu J, Li CH; L-Editors: McRae M, Song LP; T-Editor: Jia Y